Streaming instability of slime mold amoebae: An analytical model

Thomas Höfer[1,2] and Philip K. Maini[1]

[1]*Centre for Mathematical Biology, Mathematical Institute, University of Oxford, 24-29 St. Giles',*
Oxford OX1 3LB, United Kingdom

[2]*Max-Planck-Institut für Physik komplexer Systeme, Bayreuther Strasse 40, D-01187 Dresden, Germany*

During the aggregation of amoebae of the cellular slime mould *Dictyostelium*, the interaction of chemical waves of the signaling molecule cAMP with cAMP-directed cell movement causes the breakup of a uniform cell layer into branching patterns of cell streams. Recent numerical and experimental investigations emphasize the pivotal role of the cell-density dependence of the chemical wave speed for the occurrence of the streaming instability. A simple, analytically tractable, model of *Dictyostelium* aggregation is developed to test this idea. The interaction of cAMP waves with cAMP-directed cell movement is studied in the form of coupled dynamics of wave front geometries and cell density. Comparing the resulting explicit instability criterion and dispersion relation for cell streaming with the previous findings of model simulations and numerical stability analyses, a unifying interpretation of the streaming instability as a cAMP wave-driven chemotactic instability is proposed. [S1063-651X(97)14408-7]

PACS number(s): 87.22.−q

I. INTRODUCTION

Spontaneous symmetry breaking under nonequilibrium conditions is characteristic of a wide variety of physical and chemical systems; it is found in areas as diverse as fluid flow, nonlinear optics, and oscillations and waves in chemical reactions [1]. On the other hand, conclusive evidence for such processes to underly spatial patterning in biological systems is relatively rare (cf. [2]). The amoeboid microorganism *Dictyostelium discoideum* has long been considered a paradigm for the study of biological pattern formation, and recently a mechanism of self-organized patterning akin to those in inanimate systems has been implicated in a morphological transition in its life cycle. When switching from unicellular to a multicellular mode of existence, cell aggregates emerge from an initially uniform layer of single cells, forming a pattern of dense cell streams which coalesce into aggregation centers [Fig. 1(a)]. A range of mathematical models based on experimentally established single-cell properties has been employed to investigate the mechanism of cell streaming [3–8]. Numerical simulations of these models demonstrate that aggregation via cell streaming is the result of an interaction of reaction-diffusion waves of an intercellular signaling molecule, cyclic adenosine 3′5′-monophosphate (cAMP), with chemically directed cell movement (chemotaxis).

In the simulations, it appears that this interaction causes an instability of wave propagation through the uniform cell layer that underlies the formation of the stream pattern. Vasiev *et al.* [4] suggest that the dependence of the cAMP wave speed on cell density plays a crucial role in the instability mechanism. This assertion is substantiated by recent results of Van Oss *et al.* [7] that show failure of cell streaming in the absence of such a dependence in the model and provide experimental evidence of its existence in the *in vivo* system. However, the model results are not conclusive, as they are obtained from numerical simulations only, and the potential influence of various factors is difficult to discern.

In order to expose the instability mechanism, linear sta-

bility analysis of traveling wave solutions to aggregation models has been attempted in [5,9]; owing to the structure of the underlying models, both are essentially numerical. Apart from the common conclusion that there is a "cell streaming instability" transverse to the direction of wave propagation, the predictions of the two analyses are quite different. Levine and Reynolds [9] find a rather complicated spectrum of growth rates of the unstable modes, $\omega(k^2)$, with a maximum for the homogeneous mode $k=0$ and a region of complex growth rates for large enough wave numbers k, predicting modes oscillatory in time as well as in space. In contrast, Höfer *et al.* [5] obtain a real dispersion relation $\omega(k^2)$ with a single maximum at nonzero k. Despite a number of approximations made, the predicted dominant wave number compares quantitatively with the dominant wave number of the emerging stream pattern in model simulations. However, the findings in [4,7] appear not to be captured by the analysis in [5], as no provision is made for the cell density dependence of the cAMP wave speed.

The purpose of the present paper is twofold. First, we translate the suggestion by Vasiev *et al.* [4] and Van Oss *et al.* [7] into a comparatively simple model of the cAMP wave cell interaction. The model is developed as an approximation to existing models of aggregation, with the advantage of allowing both traveling wave solutions and their stability to be established analytically. Second, we use the explicit results on the parameter dependence of the streaming instability obtained to reexamine the previous interpretations of the instability mechanism suggested by simulation studies and (numerical) linear stability analyses.

Following a brief review of the cell biology and the existing models of *Dictyostelium* aggregation in Sec. II, in Sec. III we derive the model of the cAMP wave cell interaction. The derivation exploits a geometrical representation of the cAMP waves as cAMP concentration contours, which is coupled with the dynamics of chemotaxis. The explicit linear stability analysis of its traveling wave solutions is carried out in Sec. IV. In Sec. V, these results are contrasted with the numerical results obtained on aggregation in the different models and the framework and results of the previous stabil-
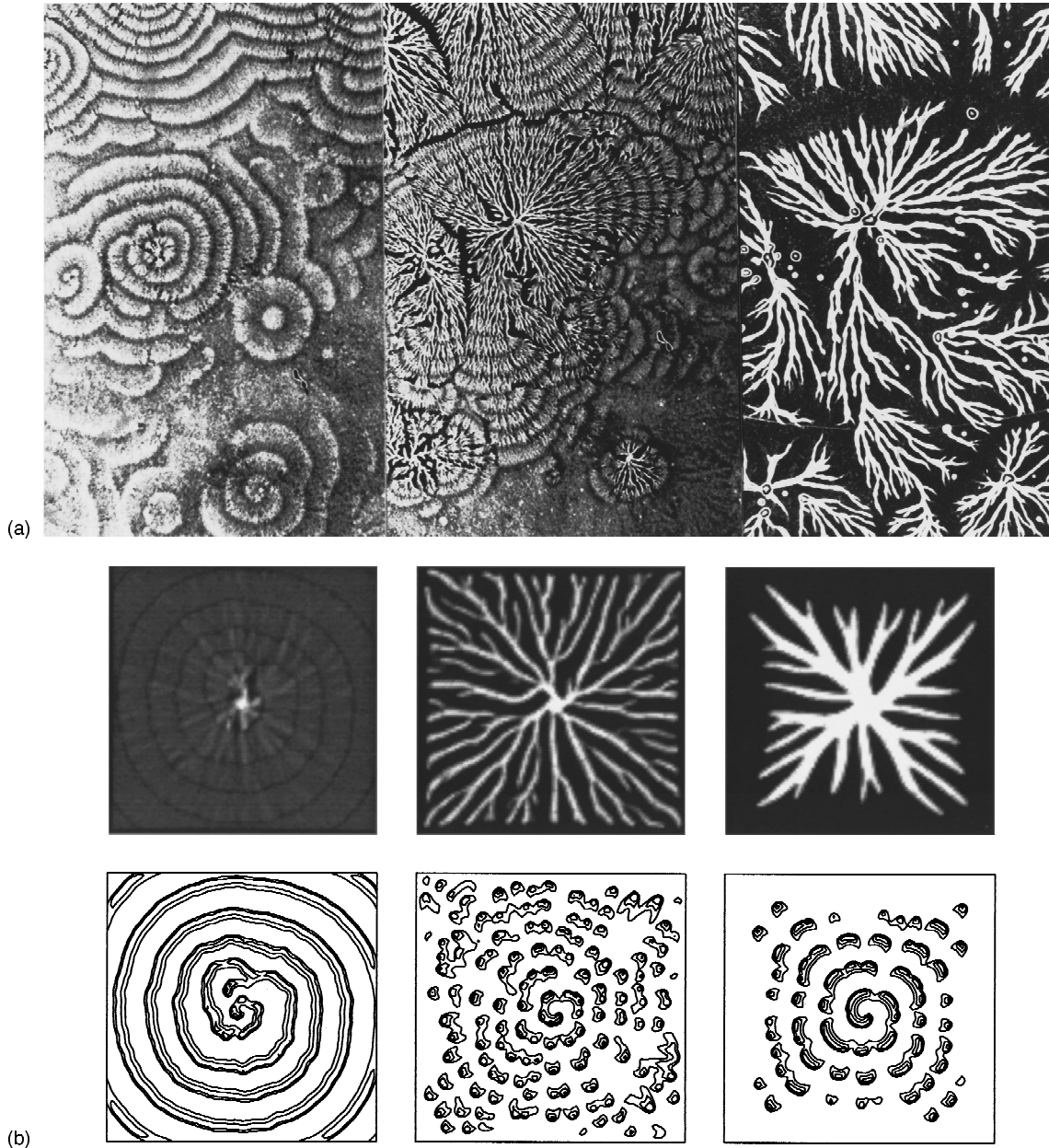
FIG. 1. Aggregation pattern of *Dictyostelium discoideum in vivo* (a) and in a model simulation (b). (a) Left: initial stage (cell density is essentially homogeneous, and white regions correspond to moving amoebae, marking the position of cAMP wave fronts; in darker regions, amoebae are stationary). Middle and right: developed cell streams $\sim$60 and $\sim$120 min later, respectively (dark regions in this photograph are depleted of amoebae). The size of the field shown is approximately 1.5 cm$\times$1.5 cm (courtesy of P. Newell). (b) Simulation of systems (1)–(3). Upper panel: cell density n (black, low; white, high). Lower panel: corresponding cAMP concentration contours u. Domain size 0.8 cm$\times$0.8 cm; snapshots taken at 15, 80, and 140 min. Parameters and functional forms: $\alpha(n) = n/(1.2 - n)$ for $0 < n < 1$ and $\alpha(n) = 5$ for $n > 1$, $\lambda f(u,v) = 90(0.2v + v^2)(0.014 + u^2)/(1 + u^2)$, $D = 1$, $g(u,v) = 2.5[1 - (1+u)v]$, $\mu = 0.012$, $\chi(v) = 0.5$, for space, time, cell density, and concentration scales of 200 μm, 4 min, 7.5$\times$10^5 cells/cm^2, and 0.5 μM, respectively (for details, see [16]). Initial conditions were a uniform cell distribution of 0.7, randomly perturbed by up to $\pm$5% at each mesh point, and a planar cAMP wave with a free tip. Note the persistence of the resulting spiral wave geometry even after breakup of the continuous front contour. Numerical scheme: ADI for diffusion, first-order upwind scheme for chemotaxis, reaction terms explicit, 201$\times$201 mesh points.

ity analyses. The comparison yields a unifying picture of the streaming instability.

II. BIOLOGY AND MODELS OF AGGREGATION

Dictyostelium discoideum belongs to a group of microorganisms that show aggregation of single cells to form cellular aggregates at some phase in their life cycles [10]. In *Dictyostelium*, multicellular development is induced by lack of nutrients and leads, via the aggregation of up to 10^5 cells, to the formation of a motile sluglike organism, eventually transforming into a fruiting body.

The process of aggregation has been described in detail (cf. [11] and references therein). Following starvation, amoebae acquire the ability to respond to extracellular stimulation by cAMP with intracellular synthesis and secretion of cAMP
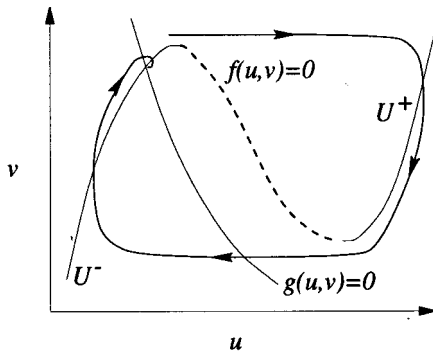
FIG. 2. Sketch of phase plane of the local kinetics of Eqs. (1) and (2), with $n = n_0$. The solid portions $U^{\pm}$ of the f-nullcline are stable, in the sense that nearby trajectories remain close. The dashed portion is unstable.

(''autocatalysis'') and also with chemotactic movement towards increasing cAMP concentration. Concomitantly, cAMP-degrading enzymes are expressed and secreted. At the onset of aggregation, concentric and spiral waves of cAMP are observed in the layer of amoebae. In the cAMP gradients of the wave fronts, cell movement towards the centers of the wave patterns takes place, alternating with a stationary phase in the wave backs and in between waves [12,13]. Typical cAMP wave speeds c are significantly larger than the maximum cell speed w_0 ($c \approx 200$–600 μm/min, $w_0 \approx 20$–30 μm/min), and consequently, the initially uniform cell density away from the aggregation centers remains practically undisturbed by chemotaxis [14]. However, cell movement subsequently ceases to be ''slaved'' by the cAMP waves. Rather than simply collecting at the aggregation centers, amoebae organize in a pattern of branching cell streams, in which they establish cell-cell contacts—a crucial process for postaggregative development [15]. This breakup of the cell layer becomes visible after the passage of about 10–20 cAMP wave fronts, with a typical wave period of 5–8 min [Fig. 1(a)].

A minimal mechanistic model of the aggregation process includes (i) the local kinetics and diffusion of the external signal, extracellular cAMP, (ii) the motile cell response towards cAMP, and (iii) the cell-internal dynamics of sensing cAMP, involving fast processes of signal relay to cAMP synthesis and motile machinery that can be eliminated adiabatically, and slow processes changing the sensitivity of an amoeba towards the cAMP signal (desensitization). Denoting by $u(x,y,t)$, $v(x,y,t)$, and $n(x,y,t)$ the concentration of extracellular cAMP, the fraction of active cAMP cell membrane receptors per cell and the cell density (number of cells per area), respectively, the model can be cast in the form [5]

$$\frac{\partial u}{\partial t} = \lambda \alpha(n) f(u,v) + D \nabla^2 u, \qquad (1)$$

$$\frac{\partial v}{\partial t} = g(u,v), \qquad (2)$$

$$\frac{\partial n}{\partial t} = \mu \nabla^2 n - \nabla \cdot [\chi(v) n \nabla u], \qquad (3)$$

where $\nabla \equiv (\partial/\partial x, \partial/\partial y)$. Briefly, $f(u,v)$ is the rate of cAMP synthesis and degradation per cell; it depends on cAMP and on the sensitivity of the cell towards cAMP stimulation,

measured by v. The total production per unit area depends on the cell density, with $\alpha(n)$ being an increasing function of n [4,5,16]. Upon sensing of cAMP, amoebae exhibit desensitization through conversion of the cAMP receptor in an inactive form (and similar effects on other molecular components of the cAMP sensing system) [17–19]. The kinetics of desensitization and the recovery of the active form are given by $g(u,v)$; $\lambda \approx 100$ is the ratio of the characteristic rates for cAMP synthesis and receptor desensitization. The dynamics of the cell distribution is governed by the advection-diffusion equation (3) [20], accounting for random cell movement with ''diffusivity'' μ, and chemotactic movement in response to cAMP with velocity $\mathbf{w} = \chi(v) \nabla u$. Here again the response depends on the cellular sensitivity with $\chi(v)$ being an increasing function of v [21,22]. The studies of Vasiev et al. [4] and Höfer et al. [5,6] employ models of the types (1)–(3), the first one with standard Fitzhugh-Nagumo excitable dynamics and the latter two with a simplified version of the cAMP kinetics derived from a detailed model of cAMP signaling [23].

An alternative approach consists in replacing Eq. (3) by the dynamics of discrete, particle like, cells equipped with internal cAMP dynamics and a chemotactic movement rule [3,7,8]. In some of this work, the dynamics of cAMP signal transduction have been modeled in more detail than Eqs. (1) and (2), by introducing evolution equations for a greater number of intracellular variables.

These aggregation models were preceded by models focusing exclusively on the cAMP wave phenomena [23–26]. Neglecting the cell density dynamics, the cAMP dynamics were considered on an idealized stationary cell layer (a reasonable approximation for the very beginning of aggregation), and therefore these investigations serve as a reference point for the analysis of Eqs. (1)–(3). Specifically, it was shown that a systematic reduction of a detailed biochemical model yields the two-variable system (1) and (2) (with $n = n_0$, a constant) [23]. The kinetics $f(u,v)$ and $g(u,v)$ arising in this reduced model are of standard excitable type (Fig. 2. Below we will exploit this general property of Eqs. (1) and (2) without resorting to detailed algebraic expression for $f(u,v)$ and $g(u,v)$.

In numerical simulations based on those biochemical rate laws and parameter estimates from experimental data, one finds concentric waves emanating from a periodic pacemaker and spiral wave solutions that closely match the cAMP waves observed at the beginning of aggregation in experiments [24]. These wave patterns appear to be stable asymptotic states of the dynamics, as is observed in a host of other excitable media of physical or chemical origin [27]. However, the recent simulations of the aggregation model (1)–(3) and related models exhibit a slow transient, relative to the time scale of wave propagation, in the course of which the cell distribution undergoes a breakup transverse to the cAMP wave fronts, accompanied by distortion and breakup of the cAMP waves. A representative example is depicted in Fig. 1(b). It clearly shows how the breakup leads to the formation of the cell stream pattern seen in vivo. Thus the numerical results strongly suggest that the combined dynamics of cAMP waves and cell movement give rise to an instability

which causes the growth of small initial perturbations of the uniform cell distribution [in the case of Fig. 1(b)] or the other variables.

Linear stability analysis of periodic wave solutions of Eqs. (1)–(3) should expose such an instability. Before proceeding to construct a specific model incorporating the wave speed hypothesis of [4,7], we outline the principle of such an analysis (e.g., [28]). For simplicity, we focus on the stability of planar periodic waves of the aggregation model [far from the center of the wave pattern, both concentric waves originating from a periodic pacemaker and spiral waves will appear as (locally) planar periodic waves]. Consider a system of evolution equations $\partial \mathbf{u}/\partial t = \mathbf{F}(\nabla^2 \mathbf{u}, \nabla \mathbf{u}, \mathbf{u})$ on an infinite two-dimensional domain $(x,y) \in (-\infty,\infty) \times (-\infty,\infty)$. Let $\mathbf{U}(z)$ denote a planar periodic traveling wave solution with period Λ and wave speed c; $z = x - ct$ denotes the appropriate traveling coordinate frame. Consider a small perturbation about $\mathbf{U}$, of the form $\mathbf{a}(z)\exp\{\omega t + iky\}$. Then the evolution of $\mathbf{a}$ will be governed by the linear system, arising from the linearization of $\mathbf{F}$ about $\mathbf{U}$, $d\mathbf{a}/dz = \mathbf{A}(\mathbf{U}(z);\omega,k)\mathbf{a}$, where $\mathbf{A}(z+\Lambda) = \mathbf{A}(z)$. We require the perturbation to remain finite as $z \to \pm\infty$; standard theory then shows that $\mathbf{a}(z;\omega,k)$ itself must be Λ periodic. If there exists such a periodic solution for a pair (ω,k) with $\omega > 0$, then the underlying wave solution $\mathbf{U}$ is unstable towards a mode with wave number k in the transverse direction. If no periodic solutions exist for any positive w, then $\mathbf{U}$ is (usually) stable [29]. Let $\mathbf{\Theta}(z)$ denote a fundamental solution of the linear system. Then the existence of a periodic solution requires the period-advance mapping $\mathbf{M} = \mathbf{\Theta}(z+\Lambda)\mathbf{\Theta}(z)^{-1}$ to have at least one eigenvalue (Floquet multiplier) of unity.

In general, analytical expressions for the monodromy matrix $\mathbf{M}$ will not be available, and for Eqs. (1)–(3) not even the unperturbed state $\mathbf{U}(z)$ can be obtained explicitly. Hence the above procedure, though applicable in principle, can only be carried out using repeated numerical integration, so that the parameter dependence of a potential instability cannot easily be established (cf. [6]). (Problems of similar nature are encountered in the analysis of transverse front or pulse instabilities in chemical systems, and various attempts to circumvent these have been made [30,31].) We now derive a simplified model from Eqs. (1)–(3) which allows explicit stability calculations for its periodic wave solutions.

III. GEOMETRICAL MODEL OF WAVE CELL INTERACTION

Intuitively, the interaction of cell movement dynamics and cAMP waves involves two crucial effects. First, propagation speed and amplitude of the cAMP waves will depend on the local cell density. This may be important, as small deviations from the average uniform density will always be present. Second, these inhomogeneities will in turn feed back into cell movement (determining the cell distribution), as cells will be attracted by the local peaks in the cAMP landscape. To describe this interaction, the details of the u and v fields are not strictly necessary; in principle, the knowledge of the u-concentration contours of the wave fronts and their cell density dependence would be sufficient. Exploiting the disparate time scales of the u and v kinetics, the problem of wave motion can be reduced to the motion of

interfaces with rapidly changing values of u (wave fronts and wave backs), joining regions of practically constant, high, or low values of u (U^+ and U^- in Fig. 2) [32]. For the motion of the wave fronts, one obtains a parabolic eikonal equation; in two dimensions, it reads

$$c_n = c - DK. \tag{4}$$

Here c, c_n and K denote the speed of a planar front, the normal speed of a curved front and the local curvature, respectively. To construct a model of aggregation, we use Eq. (4) in place of Eqs. (1) and (2) and couple it with the chemotaxis equation (3) via a modified "chemotaxis rule." The cell-density dependence of cAMP synthesis, $[\alpha(n)]$, will result in a "constitutive relation" $c(n)$.

For wave fronts that are close to a planar front, we can orient the coordinate system such that the front position is described by $x = \bar{x}(y,t)$; we write $\bar{x}$ to distinguish the front position from the independent space variable. In this case, using the standard expressions for curvature and normal of a curve $(x(t),y(t))$, the eikonal equation (4) can be recast in the form

$$\bar{x}_t = \frac{D\bar{x}_{yy}}{1+\bar{x}_y^2} + c\sqrt{1+\bar{x}_y^2}. \tag{5}$$

Clearly, this is solved by a planar wave, $\bar{x}(t) = x_0 + ct$. In the original derivation, Eq. (5) describes the narrow, "boundary layer" wave front, with a typical width of order λ^{-1} in the appropriate scaling. Here we will relax this interpretation and assume *all* u contours to obey Eq. (5). This trivially holds for a planar front, and as we will be concerned with small perturbations around planar waves, this assumption appears reasonable. Thus Eq. (5) now defines a continuous field of u contours. To make this idea explicit, we interpret x_0 as a parameter specifying the concentration contour, and thus for each contour we have $\bar{x} = \bar{x}(x_0,y,t)$. Specifically, we may choose the parametrization $x_0 = x$. Introducing the traveling frame $z = x + ct$, we transform from (x,y,t) to (z,y,t) coordinates, to obtain

$$\bar{x}_t = -c\bar{x}_z + \frac{D\bar{x}_{yy}}{1+\bar{x}_y^2} + c\sqrt{1+\bar{x}_y^2}. \tag{6}$$

This equation has the plane wave solution $\bar{x} = z$, representing a continuum of parallel contour lines, parametrized by the traveling wave coordinate, which are stationary in the z frame.

The evolution of the cell density is governed by Eq. (3). In the present model, we replace the specific choice of the chemotactic cell velocity, $\mathbf{w} = \chi(v)\nabla u$, with a similar "chemotaxis rule" using the cAMP front contours. Transformation of Eq. (3) to (z,y,t) coordinates yields

$$n_t = \mu(n_{zz} + n_{yy}) - cn_z - (\partial_z,\partial_y)\cdot(n\mathbf{w}). \tag{7}$$

The orienting influence of the cAMP gradient and the periodic character of cell movement are encapsulated in the following definition for $\mathbf{w}$. When a specific cAMP contour $\bar{x}_f$, marking the beginning of a wave front, reaches a location in the field of amoebae, the amoebae at this location start to move with constant speed w_0 for a fixed time interval Δt, being equal to the duration of the wave front, perpendicular to the cAMP contours:

$$\mathbf{w}(\overline{x}(z,y,t)) = \begin{cases} \dfrac{w_0}{\sqrt{1+\overline{x}_y^2}} \begin{pmatrix} 1 \\ -\overline{x}_y \end{pmatrix} & \text{for } \overline{x}_f \leq z < \overline{x}_f + c\Delta t, \\ 0 & \text{otherwise.} \end{cases}$$

(8)

Finally, the local wave speed in Eq. (6) will be a function of the cell density,

$$c = c(n).$$ (9)

In models of the type (1)–(3), $c(n)$ is monotonically increasing. However, in more complex models employing detailed intracellular dynamics, one can find more complicated relationships, typically showing an increasing $c(n)$ for small densities with a slight decrease or an approximately constant region for higher values of n [7,25]. The experimental results in [7] show an increase with cell density. However, wave speed was only measured for two different densities and so it is difficult to infer a continuous relationship $c(n)$.

Equations (6)–(9) constitute the model of the cell wave interaction. It is possible to obtain order-of-magnitude estimates of the parameters from the experimental literature. We have $c \approx 400$ μm/min, $w_0 \approx 20$ μm/min, $D \approx 10^4$ μm^2/min, and $\mu \approx 70$ μm^2/min (cf. [6]); with space and time scales of 200 μm and 5 min, respectively, this gives $c_0 = 10$, $w_0 = 0.5$, $D = 1$, and $\mu = 10^{-2}$.

Planar periodic traveling waves (X,N) are y- and t-independent solutions of system (6)–(9). Neglecting fast-decaying exponentials associated with the smallness of μ, they take the form

$$X(z) = z \,(\text{mod } \Lambda),$$ (10)

$$N(z) = \begin{cases} n_1 \equiv n_0/(1+w_0/c) & \text{for } 0 \leq z\,(\text{mod } \Lambda) < z_1, \\ n_0 & \text{for } z_1 \leq z\,(\text{mod } \Lambda) < \Lambda, \end{cases}$$

where $z_1 = c\Delta t$, and Λ denotes the spatial period. The locations of the wave fronts are taken to be $z = j\Lambda$, $j = 0, \pm 1, \pm 2, \ldots$. In addition, define

$$W(z) = \begin{cases} w_0 & \text{for } 0 \leq z\,(\text{mod } \Lambda) < z_1, \\ 0 & \text{for } z_1 \leq z\,(\text{mod } \Lambda) < \Lambda. \end{cases}$$ (11)

Clearly, the uniform density is only insignificantly perturbed by the wave fronts.

IV. INSTABILITY OF PLANAR WAVES

Now introduce the perturbation of the planar wave solution $\overline{x}(z,y,t) = X(z) + \hat{x}\exp\{\omega t + iky\}$, $n(z,y,t) = N(z) + \hat{n}(z,y,t)\exp\{\omega t + iky\}$. Relation (9) is simply expanded $c = c_0(n_0) + c_1(n_0)\hat{n}$, where we take the coordinate frame to move with c_0, $z = x + c_0 t$. From direct simulations of Eqs. (1)–(3), we can estimate $c_1 \approx 5$ for the parameter set of Fig. 1(b) [16]. In a first approximation, we assume that cell movement still sets in at $z = j\Lambda$, irrespective of perturbations of the fronts. Under this assumption, we obtain the following linear system for $(\hat{x},\hat{n})$:

$$\frac{d}{d\xi}\begin{pmatrix} \hat{x} \\ (1+W(\xi)/c_0)\hat{n} \end{pmatrix} = \begin{pmatrix} -\omega - k^2 D & c_1 \\ k^2 W(\xi)N(\xi) & -\omega - k^2\mu \end{pmatrix}\begin{pmatrix} \hat{x} \\ \hat{n} \end{pmatrix},$$ (12)

where we have rescaled $z = c_0\xi$. Noting that $\mu/c_0^2 \ll 1$, we have neglected the term

$$-\frac{\mu}{c_0^2}\frac{d^2}{d\xi^2}\begin{pmatrix} 0 \\ \hat{n} \end{pmatrix}$$

on the right-hand side of Eq. (12). It can be shown that this perturbation, albeit singular, retains the solutions relevant for the stability of underlying wave solutions in the perturbed system (12) [28]. In addition, we verified in sample calculations that the effect of the perturbation on the solutions of Eq. (12) is indeed small [16].

Equation (12) has the principal structure $d\mathbf{u}/d\xi = \mathbf{A}^+\mathbf{u}$ for $\xi \in I_j^+$ and $d\mathbf{u}/d\xi = \mathbf{A}^-\mathbf{u}(\xi)$ for $\xi \in I_j^-$, where $I_j^+ = (j\Lambda,(j+\alpha)\Lambda)$, $I_j^- = ((j+\alpha)\Lambda,(j+1)\Lambda)$, $j = 0,1,2,\ldots$, $\alpha \equiv z_1/\Lambda$, and $\mathbf{A}^\pm$ are constant regular matrices. This special, piecewise constant, case of a linear system with periodic coefficients can be treated analytically as follows. Denote the fundamental solutions for the $I^\pm$ intervals by $\mathbf{\Theta}^\pm$. They have the form $\mathbf{\Theta}^\pm(\xi) = \mathbf{Z}^\pm\text{diag}\{e^{\lambda_i^\pm\xi}\}\mathbf{C}^\pm$, where $\mathbf{Z}^\pm$ and $\lambda_i^\pm$ are the matrices of eigenvectors and corresponding eigenvalues, respectively; $\mathbf{C}^\pm$ are constant matrices. The fundamental solution for a complete period Λ can be found by matching these at $\xi = (j+\alpha)\Lambda$, requiring $\mathbf{\Theta}^+((j+\alpha)\Lambda) = \mathbf{\Theta}^-((j+\alpha)\Lambda)$. From this one obtains the monodromy matrix $\mathbf{M} = \mathbf{\Theta}(z+\Lambda)\mathbf{\Theta}(z)^{-1}$, as

$$\mathbf{M} = (\mathbf{Z}^+\mathbf{C}^+)^{-1}\mathbf{Z}^-\text{diag}\{e^{\lambda_i^-(j+1)\Lambda}\}$$

$$\times [\mathbf{Z}^-\text{diag}\{e^{\lambda_i^-(j+\alpha)\Lambda}\}]^{-1}\mathbf{Z}^+\text{diag}\{e^{\lambda_i^+(j+\alpha)\Lambda}\}\mathbf{C}^+. \quad (13)$$

For Eq. (12) there exists a straightforward correspondence between the spectrum of (maximal) growth rates $\omega(k^2)$ and the spectrum of maximal Floquet multipliers, $\sigma(\omega,k^2)$, which allows the stability properties of system to be established in a compact manner. Realizing that the monodromy matrix has the structure $\mathbf{M} = \mathbf{M}_0\exp\{-\omega\Lambda\}$, where $\mathbf{M}_0$ is the monodromy matrix corresponding to $\omega = 0$, one can easily show that

$$\omega(k^2) = \Lambda^{-1}\ln\sigma(0,k^2).$$ (14)

Hence all we need to calculate is the spectrum of $\mathbf{M}_0$ from Eqs. (10) and (13). One of the two eigenvalues lies always in the interval $(-1,1)$, while the modulus of the other,

$$\sigma(0,k^2) = \tfrac{1}{2}[\text{tr}\mathbf{M}_0 + (\text{tr}^2\mathbf{M}_0 - 4 \,\det\mathbf{M}_0)^{1/2}],$$ (15)

can be greater than 1. One obtains $\text{tr}\mathbf{M}_0 = [k^2(\lambda_1^+ - \lambda_2^+)(\mu - D)]^{-1}[(\lambda_1^+ + k^2 D)(\lambda_2^+ + k^2\mu)(e^{(\lambda_1^+ - k^2\mu)\alpha\Lambda} + e^{(\lambda_2^+ - k^2 D)\alpha\Lambda}) - (\lambda_1^+ + k^2\mu)(\lambda_2^+ + k^2 D)(e^{(\lambda_1^+ - k^2 D)\alpha\Lambda} + e^{(\lambda_2^+ - k^2\mu)\alpha\Lambda})]$, $\det\mathbf{M}_0 = \exp\{-k^2(\mu+D)\Lambda\}$, and $\lambda_{1,2}^+ = \tfrac{1}{2}\{-k^2(D+\mu) \pm [k^4(D-\mu)^2 + 4k^2 c_1 w_0 n_1]^{1/2}\}$. Inserting these expressions in Eq. (15), one can show that a positive growth rate $\omega(k^2)$ is obtained if and only if

$$\text{tr}\mathbf{M}_0 > 1 + \det\mathbf{M}_0.$$ (16)

This implies that an instability is associated with σ passing through 1 and, consequently $\omega(k^2)$ being always real, predicting the growth of a stationary pattern transverse to the wave fronts. The homogeneous mode $k = 0$ is always a neutral mode, due to the conservation of total cell number. Thus we can expect an instability to set in at large wavelengths,

and expanding Eq. (16) about $k^2=0$, one finds that the periodic waves are unstable towards large wavelengths for $c_1 n_1 w_0 > 0$ and stable for $c_1 n_1 w_0 \leq 0$. Hence, in this simplified model, the presence of chemotactic cell movement combined with a ''positive'' dependence of cAMP wave speed on cell density, $c_1 = dc(n)/dn > 0$, always leads to an instability. This result is a clear confirmation of the assertion of [4,7].

The actual range of unstable modes and associated growth rates can be inferred from the dispersion relation $\omega(k^2)$. For sufficiently large cAMP wave periods $\Lambda \gg [k^2(D+\mu)]^{-1}$, it is well approximated by

$$\omega(k^2) \approx \frac{\alpha}{2}[-k^2(D+3\mu) + \sqrt{k^4(D-\mu)^2 + 4k^2 c_1 n_1 w_0}];$$
(17)

sample calculations show that even for small k and $\Lambda = O(1)$ Eq. (17) is rather close to the actual dispersion relation (cf. Fig. 3). [In Eq. (17) was assumed that $\mu < D$ as estimated above; the relation for $\mu > D$ is found by interchanging μ and D.] Relation (17) predicts a range of unstable wave numbers $0 < k^2 < c_1 n_1 w_0/[2\mu(\mu+D)]$ with a single maximum; or, alternatively, a mode $k^2 > 0$ is unstable, if

$$c_1 w_0 n_1 > 2k^2 \mu(\mu+D),$$
(18)

and stable otherwise. Typical dispersion relations are shown in Fig. 3.

For realistic parameter values ($c_1 = 5$, $n_1 = 1$, $w_0 = 0.5$), we have a maximum growth rate of about 0.19 (or 0.04 min^{-1}) and a dominant wave number of ~ 3.7 (or a wavelength of 340 μm). Given a typical cell diameter of about 10 μm, the analysis thus predicts the formation of clusters of a few cells. This happens on a relatively slow time scale; the linear doubling time of the patterning amplitude is equivalent to the passage of three to four cAMP pulses.

V. DISCUSSION

A. Comparison with model simulations

The analysis can be thought of as investigating a situation in which stable periodic waves exist (e.g., for $w_0 = 0$) and then a parameter is switched to render the waves unstable ($w_0 > 0$). The natural situation of aggregation is of course somewhat different. Here the waves are ''switched on'' and start to propagate from distinct sources, and the combined dynamics of cAMP signaling and cell movement are unstable from the outset. Therefore the instability develops as the wave patterns expand. It will become visible first in the neighborhood of the aggregation centers, propagating outwards with the waves. This conjecture is borne out both by experiments and model simulations [Figs. 1(a) and 1(b), respectively].

The stability analysis is confined to patterning perpendicular to the direction of wave propagation and does not address the issue of pattern selection on the two-dimensional domain. However, it is intuitive that the distortions of the wave fronts cause continuous cell streams to form. The presence of a dominant wave number provides a recipe for a branching network of cell streams in the quasicircular geometry of an aggregation territory. Evidence of a dominant spa-
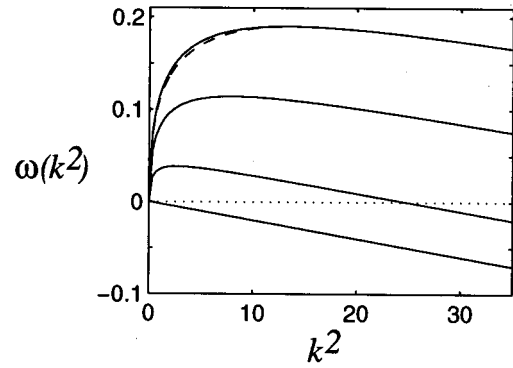
FIG. 3. Dispersion relations, $\omega(k^2) = \Lambda^{-1} \ln \sigma(0,k^2)$, for $\Lambda = 2$, $\alpha = 0.1$, $\mu = 0.01$, $D = 1$, and in ascending order $c_1 n_1 w_0 = 0$, 0.5, 1.5, and 2.5. The dashed curve shows the approximation (17) for $c_1 n_1 w_0 = 2.5$.

tial wavelength of the emerging stream pattern has been obtained in model simulations [6,16]. The model simulations appear to match the experimental results, but a quantitative analysis of the experimental patterns is lacking at present.

B. Comparison with previous stability analyses

Starting from a rather different set of assumptions, the model (6)–(9) yields essentially the same dispersion relation as the previous analysis in [6]. The analysis of [6] did not incorporate wave front curvature explicitly; it was based on following the amplitudes of u, v, and n in Eqs. (1)–(3) perpendicular to the direction of wave propagtion as a perturbation of the periodic planar wave is being introduced. The close correspondence between the results of the two analyses also extends to the instability criteria. By means of a rough, qualitative, ''caricature'' of the numerical stability calculations of Eqs. (1)–(3), in [6] the following instability criterion was derived: Periodic waves are unstable if

$$p n_0 \chi_0 > 2\mu(k^2 D + \gamma n_0).$$
(19)

Here p, n_0, χ_0, and γ denote a measure of the production rate of cAMP, the unperturbed initial cell density, the chemotactic coefficient (being proportional to cell speed), and the degradation rate of cAMP; the meaning of μ and D is the same as in the present model. Thus in both models it is the competition between the combined effect of cAMP production and chemotactic cell movement, on the one hand, and the dissipative effects of random cell movement and cAMP diffusion [and cAMP degradation in Eq. (19)], on the other, that determines whether the streaming instability occurs.

The two approaches to stability analysis in the present paper and in [6] therefore emphasize *complementary* features of the instability mechanism, and the exclusive focus on cAMP wave front curvature in [4,7] appears somewhat one sided. For streaming to occur, it is important that local cAMP synthesis increase with cell density. This will manifest itself both in local front curvature (i.e., propagation speed) and cAMP amplitude.

It is not straightforward to see where the discrepancy with the results in [9], and in particular the very different shape of the dispersion relation, arises, since they are obtained by a

numerical procedure. In addition, the detailed forms of the chemotaxis terms differ in the models of [9,6] and the present model. In [9] separate dynamics are assumed for $\mathbf{w}$ in the wave fronts, $d\mathbf{w}/dt = -\Gamma\mathbf{w} + k\nabla u$, while in [6] $\mathbf{w} \propto \nabla u$ in the wave fronts. Here Eq. (8) corresponds essentially to $\mathbf{w} = w_0 \nabla u / \|\nabla u\|$. Hence in all three models the direction of cell movement follows the cAMP gradient, but in the present model the speed is constant rather than gradient dependent. (This latter assumption in the present model is forced by the contour description of the cAMP waves which retains the direction but not the magnitude of the chemical gradients; a constant ''intrinsic'' speed may actually be more realistic biologically.) This may account for differences in detail. However, the agreement of the results of the present analysis with that of [6] together with the evidence from model simulations argues strongly in favor of a generic single-humped dispersion relation.

C. Conclusion

The ''pattern'' of the instability criteria (18) and (19) emphasizes the connection of the streaming instability with the chemotactic instability found in a simpler system by Keller and Segel [33]. [In the Keller-Segel system, actively moving particles, such as cells (described by a continuous density), collect in clusters separated by a characteristic distance by responding chemotactically to a signal they emit in a continuous fashion.] In this sense, the streaming instability is a chemical-wave-driven chemotactic instability. This is further underlined by another feature of aggregation, namely, the progressive ''coarsening'' of the initial pattern, seen both *in vivo* and in model simulation (cf. Fig. 1). Such a coarsening has also been observed in simulations of a discrete-particle analog of the Keller-Segel system [34]. Similar phenomena are found in other types of aggregative patterning, such as dendritic growth [35].

Recently, there have been experimental studies of other microbial systems in which chemotactic instabilities are likely to be involved in the formation of collective cell patterns [36–38]. Moreover, the modeling approach presented here may be applied to other excitable systems in which wave propagation alters the state of the medium.

[1] M. C. Cross and P. C. Hohenberg, Rev. Mod. Phys. **65**, 851 (1993).
[2] T. Höfer and P. K. Maini, Nature (London) **380**, 678 (1996).
[3] D. A. Kessler and H. Levine, Phys. Rev. E **48**, 4801 (1993).
[4] B. N. Vasiev, P. Hogeweg, and A. V. Panfilov, Phys. Rev. Lett. **73**, 3173 (1994).
[5] T. Höfer, J. A. Sherratt, and P. K. Maini, Proc. R. Soc. London, Ser. B **259**, 249 (1995).
[6] T. Höfer, J. A. Sherratt, and P. K. Maini, Physica D **85**, 425 (1995).
[7] C. Van Oss, A. V. Panfilov, P. Hogeweg, F. Siegert, and C. J. Weijer, J. Theor. Biol. **181**, 203 (1996).
[8] J. Dallon and H. G. Othmer, Philos. Trans. R. Soc. London, Ser. B **352**, 391 (1997).
[9] H. Levine and W. Reynolds, Phys. Rev. Lett. **66**, 2400 (1991).
[10] J. T. Bonner, *Life Cycles* (Princeton University Press, Princeton, 1994).
[11] P. N. Devreotes, Science **245**, 1054 (1989).
[12] K. J. Tomchik and P. N. Devreotes, Science **212**, 443 (1981).
[13] F. Siegert and C. J. Weijer, in *Oscillations and Morphogenesis*, edited by L. Rensing (Dekker, New York, 1993), pp. 133–152.
[14] F. Alcantara and M. Monk, J. Gen. Microbiol. **85**, 321 (1974).
[15] L. Desbarats, S. K. Brar, and C. H. Sin, J. Cell. Sci. **107**, 1705 (1994).
[16] T. Höfer, Ph.D thesis, University of Oxford, 1996.
[17] P. J. Van Haastert, M. Wang, A. A. Bominaar, P. N. Devreotes, and P. Schaap, Mol. Biol. Cell **3**, 603 (1992).
[18] Y. H. Tang and H. G. Othmer, Math. Biosci. **120**, 25 (1994).
[19] A. Goldbeter, *Biochemical Oscillations and Cellular Rhythms* (Cambridge University Press, Cambridge, England, 1996).

[20] C. S. Patlak, Bull. Math. Biophys. **15**, 311 (1953).
[21] T. Höfer, P. K. Maini, J. A. Sherratt, M. A. J. Chaplain, P. Chauvet, D. Metevier, P. C. Montes, and J. D. Murray, Appl. Math. Lett. **7**, 1 (1994).
[22] R. E. Goldstein, Phys. Rev. Lett. **77**, 775 (1996).
[23] J. L. Martiel and A. Goldbeter, Biophys. J. **52**, 807 (1987).
[24] J. J. Tyson, K. A. Alexander, V. S. Manoranjan, and J. D. Murray, Physica D **34**, 193 (1989).
[25] P. B. Monk and H. G. Othmer, Proc. R. Soc. London, Ser. B **240**, 555 (1990).
[26] Y. H. Tang and H. G. Othmer, Philos. Trans. R. Soc. London, Ser. B **349**, 179 (1995).
[27] R. Kapral and K. Showalter, *Chemical Waves and Patterns* (Kluwer, Dobrecht, 1995).
[28] K. Maginu, J. Diff. Eqns. **39**, 73 (1981).
[29] D. H. Sattinger, Adv. Math. **22**, 312 (1976).
[30] D. Horvath, V. Petrov, S. K. Scott, and K. Showalter, J. Chem. Phys. **98**, 6332 (1993).
[31] A. Hagberg and E. Meron, CHAOS **4**, 477 (1994).
[32] J. P. Keener, SIAM (Soc. Ind. Appl. Math.) J. Appl. Math. **46**, 1039 (1986).
[33] E. F. Keller and L. A. Segel, J. Theor. Biol. **26**, 399 (1970).
[34] F. Schweitzer and L. Schimansky-Geier, Physica A **206**, 359 (1994).
[35] D. A. Kessler, J. Koplik, and H. Levine, Adv. Phys. **37**, 255 (1988).
[36] E. O. Budrene and H. C. Berg, Nature (London) **376**, 49 (1995).
[37] A. J. Shapiro, Bioessays **17**, 597 (1995).
[38] O. Raupric, M. Matsushita, C. J. Weijer, F. Siegert, S. E. Esipov, and J. A. Shapiro, J. Bacteriol. **178**, 6525 (1996).